buildings

MDPI

Article

Effects of Cover-Plate Geometry on the Mechanical Behavior of Steel Frame Joints with Middle-Flange and Wide-Flange H-Beams

Osama Zaid Yahya Al-Ansi, Linfeng Lu *, Saleem Mohammed Ali Ahmed AL-Saeedi and Bingyou Liu

School of Civil Engineering, Chang'an University, 75 Chang'an Middle Rd., Xi'an 710062, China; 2022028916@chd.edu.cn (O.Z.Y.A.-A.); 2021028918@chd.edu.cn (S.M.A.A.A.-S.); 2023228019@chd.edu.cn (B.L.)
* Correspondence: lulinfeng@chd.edu.cn

Abstract: This study investigates the mechanical behavior of cover-plate reinforced connections in steel frames with I-section columns and middle- or wide-flange H-beams, addressing gaps in current design standards. Finite element analyses validated by experimental data were employed to explore the effects of cover-plate geometry—shape, length, and thickness—on seismic performance. Results demonstrate that cover plates improve load-bearing capacity and ductility by relocating plastic hinges outward from joint regions. Specifically, cover-plate connections increased ductility by 25%, yield moment by 15%, and initial rotational stiffness by 7% compared to non-reinforced connections. The shape of the top cover plate had minimal impact on mechanical behavior. The cover-plate length and thickness significantly influenced seismic ductility and load-bearing capacity. The cover-plate thickness should be at least 0.3 times the beam flange thickness (not less than 6 mm) while ensuring the combined thickness of the cover plate and beam flange does not exceed the column flange thickness. These recommendations address the conservatism of existing standards, balancing material efficiency and seismic performance. Optimal cover-plate lengths of 0.7 to 0.9 times the beam depth were also identified. These findings provide practical guidelines for designing resilient steel frame connections in seismic regions.

Keywords: cover plate; connections; cyclic loading; H-shape beam; plastic hinge

Academic Editor: Hugo Rodrigues

Received: 1 December 2024
Revised: 6 January 2025
Accepted: 8 January 2025
Published: 11 January 2025

Citation: Al-Ansi, O.Z.Y.; Lu, L.; AL-Saeedi, S.M.A.A.; Liu, B. Effects of Cover-Plate Geometry on the Mechanical Behavior of Steel Frame Joints with Middle-Flange and Wide-Flange H-Beams. *Buildings* **2025**, *15*, 203. https://doi.org/10.3390/buildings15020203

1. Introduction

The Northridge and Kobe earthquakes occurred 40 years ago, leading to significant damage and failure of beam–column joints [1–3]. Both earthquakes revealed weaknesses in traditional welded and bolted connections in steel frames. They had a major impact on connection design standards and academic research [4]. Beam-to-column connections are crucial for steel building or rack frames [5]. Special attention is required for performance analysis under seismic, fire, and other disasters.

After the Northridge earthquake, the Federal Emergency Management Agency (FEMA) introduced new guidelines, such as FEMA-350 [6], recommending enhanced seismic design criteria for steel moment-resisting frames. This guideline emphasized increased connection toughness and reliability to withstand severe earthquake loading [6]. Similarly, in Japan, the Kobe earthquake prompted amendments to the Building Standard Law, focusing on strengthening steel structure design for improved energy dissipation and plastic deformation capacity [7]. The academic community responded by conducting experimental and analytical studies on various connection types, including reinforced connections

with welded cover plates, to understand failure mechanisms and improve seismic detailing [8,9]. Some design standards [10–12] have adopted the cover-plate connection as a post-earthquake retrofitting method for steel frame connections. Additionally, it has been incorporated as a connection method for new steel frames in FEMA-350 [6] and in the Chinese standard JGJ 99-2015 [13].

Research on the traditional form of cover-plate reinforced connections has been ongoing. I-section columns are commonly used in steel frames. However, due to inevitable defects in weak joint regions, replacing the column web or welding reinforcing plates in a certain range at the joint area is necessary [14], which complicates construction. Lu et al. proposed new joint region strengthening connections [15,16] to address this and investigated and reported on the design methods for weak-axis cover-plate connections [17]. Shi's team extended the application of cover-plate connection joints from conventional low-carbon and low-alloy steel frames to high-strength steel frames [18,19]. Their research demonstrated that cover-plate connection joints exhibit excellent seismic performance and high ductility when using high-strength steel.

Building on the traditional cover-plate connection design, some scholars have introduced improvements. For instance, Casita et al. [20] combined the traditional cover-plate connection with the reduced beam section (RBS) connection. Numerical investigations revealed that the new connection outperformed traditional cover-plate and RBS connections regarding plastic hinge location, while the cover-plate connection exhibited the best energy dissipation capacity. Meng et al. [21] introduced a new connection type featuring double-leg energy dissipation cover plates (DEDCPs) and conducted experimental and numerical studies. Their findings indicated that the hysteretic curves of the DEDCPs were well-formed and demonstrated strong energy dissipation capabilities. Ribeiro et al. [22] used the Solid Isotropic Material with Penalization (SIMP) method to study the bolt cover-plate connection used in traditional H-shaped steel beam splicing, extending the application of topology optimization techniques and exploring advanced computer-aided design technologies. Nassiraei [23] conducted a different technical exploration, where he developed a comprehensive probabilistic framework to evaluate tubular X-joint resistance strengthened with collar plates under tensile and fire conditions, integrating extensive FE analyses and advanced statistical modeling. This work is a key reference for researchers studying tubular joint behavior, offering rigorous FE analyses and advanced statistical modeling for probabilistic structural assessment under extreme conditions. Other studies have used bolt cover-plate technology to address the splicing issues of modular steel buildings. For example, Cao's team developed a module-to-module bolted connection [24–26]. Deng et al. developed a novel liftable connection [27,28]. The extensive experimental and numerical analysis results of these two new cover-plate connections are highly beneficial for promoting the adoption and use of prefabricated steel buildings.

Despite the emergence of various new cover-plate connection technologies, traditional cover-plate connections continue to dominate steel frame structures in China. The data of cover-plate connections used in the standards [12,13,29] are based on research conducted on connections of narrow-flanged H-beams ($b_f/d_b \leq 1/2$, where b_f is the beam flange width and d_b is the beam depth, as shown in Table 1). With the extensive promotion of hot-rolled H-shapes in China, middle-flange and wide-flange hot-rolled H-shapes are also used in beam components [30]. Therefore, the applicability of design standards to cover-plate connections for H-shaped beams with middle and wide flanges needs further investigation, and existing research on cover-plate connections reveals certain gaps. Existing research [31,32] has proven that reliable numerical analysis methods were used to investigate the seismic performance of joints or connections. This study uses finite element numerical methods to analyze the seismic performance of cover-plate connections between

H-shaped steel columns and H-shaped steel beams with medium and wide flanges. The results are compared with existing design criteria for cover-plate connections based on narrow-flange H-shaped beams, and new design recommendations are provided.

Table 1. List of notations and abbreviations.

Notation	Definition	Notation	Definition
b_f	beam flange width	CP	specimens with cover plates
d_b	beam depth	WCP	specimens without cover plates
x-axis	length direction of the beam	CPS	specimens with varying shapes of top cover plate
y-axis	height direction of the column	CPL	specimens with varying lengths of rectangular cover plates
z-axis	width direction of the beam	CPT	specimens with varying thicknesses of rectangular cover plates
σ_y	yield stress	b_{cp}	width of the cover plate
σ_u	maximum stress	t_{cp}	thickness of the cover plate
σ_{st}	failure stress	t_{bf}	thickness of the beam flange
ε_y	yield strain	l_{cp}	length of the cover plate
ε_u	maximum strain	b_{cp1}	width of the top cover plate
ε_{st}	failure strain	b_{cp2}	the width of the bottom cover
MPa	Mega pascal	θ_y	yield rotational displacements
R_k	initial rotational stiffness	θ_{max}	peak rotational displacements
M_y	yield moment	θ_u	terminated rotational displacements
M_{max}	peak moment	θ_p	plastic rotation capacity
M_u	terminated moment		

2. Numerical Analysis Methods and Materials

2.1. Material Property

As shown in Figure 1, the steel and bolt materials adhere to a three-line isotropic hardening model corresponding to a simplified engineering stress–strain curve. In this context, σ_y, σ_u, and σ_{st} denote the yield, maximum, and failure stresses, respectively, while ε_y, ε_u, and ε_{st} represent the corresponding strains. The properties of Q235 steel and grade 8.8 M20 bolts are from Refs. [33,34]. Table 2 displays the engineering stresses and strains of Q235 steel and an 8.8-grade bolt. The Poisson's ratio is taken as 0.3. In ABAQUS (6.1.4) analysis, it is necessary to convert engineering stress and strain into true stress and strain. The analysis applies the Mises yield criterion and mixed hardening rule reflecting the Bauschinger effect and cyclic hardening of steel.

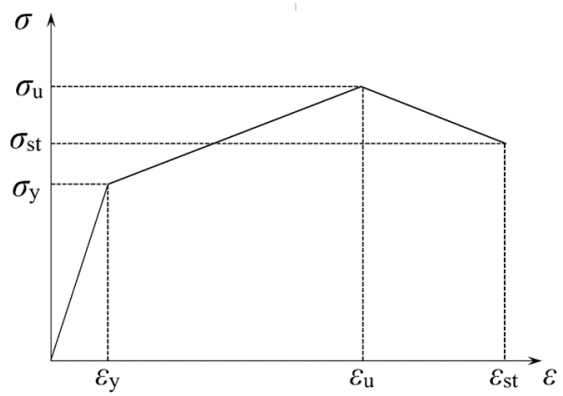

Figure 1. Three-line stress–strain relationship curve.

Table 2. Material properties of Q235 steel and 8.8 grade bolt.

Material Samples	*E*/MPa	σ_y/MPa	ε_y	σ_u/MPa	ε_u	σ_{st}/MPa	ε_{st}
Q235 steel	197,000	320	0.001748	451.667	0.14361	360.643	0.19653
8.8-grade bolt	161,000	645.0	0.004	793.5	0.025	636.9	0.121

2.2. Numerical Modeling

The T-shaped joint of the external steel frame was selected, with the beam and column lengths being 3000 mm and 3600 mm, respectively, measured from the hinge center. The skin steel plates on both sides of the reinforced joint region were 8 mm thick, with a width equal to the column depth and a height extending 150 mm above and below the beam depth, welded onto the column flanges. The calculation diagram is shown in Figure 2a.

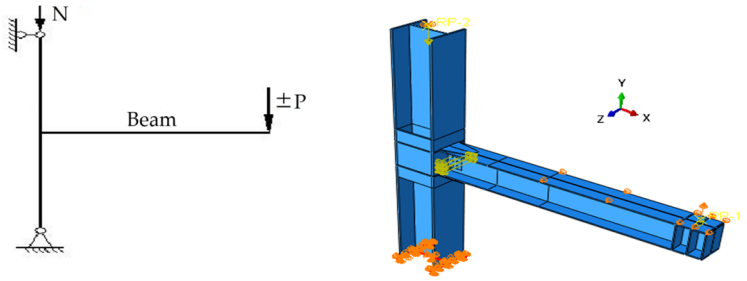

(**a**) (**b**)

Figure 2. Schematic diagram of boundary condition and node loading. (**a**) Calculation diagram; (**b**) Abaqus.

The length direction of the beam, the height direction of the column, and the width direction of the beam are defined as the *x*-axis, *y*-axis, and *z*-axis, respectively. As shown in Figure 2b, the top section of the column is coupled, with the coupling point restricted in the x and z directions for linear displacement. At the base of the column, linear displacements in all three directions are constrained while rotations are allowed. At the top of the column, only linear displacements in the x and z directions are restricted. A concentrated force was applied at the top of the column, corresponding to an axial load ratio of 0.3 to conform to the majority of middle- and top-floor joints in multi-story and high-rise steel frame buildings. Displacement coupling was applied to all nodes within a 150 mm range at the beam-end loading point, and cyclic displacement loading was used to simulate seismic effects to the coupled nodes in the y direction. The loading protocol for the specimen followed ANSI/AISC 341-05 [35], which includes six cycles at inter-story drift angles of 0.375% rad, 0.5% rad, and 0.75% rad, and four cycles at 1% rad. For drift angles of 1.5% rad, 2% rad, 3% rad, and 4% rad, two cycles were applied for each angle, with two additional cycles for every subsequent 1% rad increment. Loading was terminated when the bearing capacity decreased to 85% of the maximum load.

ABAQUS (Version 6.1.4) finite element analysis technology is well-established and reliable. The C3D8I elements, which are 8-node linear hexahedral elements with integrated hourglass control, were utilized for the structural analysis. These elements were chosen for their ability to accurately represent the geometry of the beam–column joints and the cover-plate areas, and they are well-suited for modeling solid structures. Using these elements ensures that the structural behavior is captured with high fidelity.

A mesh convergence analysis was conducted to verify the adequacy of the mesh size and ensure the accuracy of the result. The process involved testing the finite element model with progressively smaller mesh sizes and comparing key output parameters, including the load–displacement curves and stress distributions at critical locations. Convergence was achieved when further mesh refinement produced negligible changes in the results, confirming that the chosen mesh size reliably captured the structural behavior. The analysis demonstrated that the selected mesh sizes struck an optimal balance between precision and computational efficiency. During the meshing of the finite element model, finer meshes were applied at the beam–column joint, expected plastic hinge locations on the beam, and contact areas such as bolt holes and bolts. For the model, the mesh size was 25 mm for

hot-rolled H-shapes, a 10 mm mesh size was applied to the 600 mm region at the beam-to-column connection to better capture the plastic hinge zone, 5 mm for the cover and web connection plate, and 2 mm for high-strength bolts. Figure 3 illustrates the 3D finite element local model, highlighting the meshed structure, particularly the critical areas such as the beam–column joint and cover plates. Refined mesh regions were clearly marked to enhance the visualization of the meshing strategy, as shown in Figure 3c.

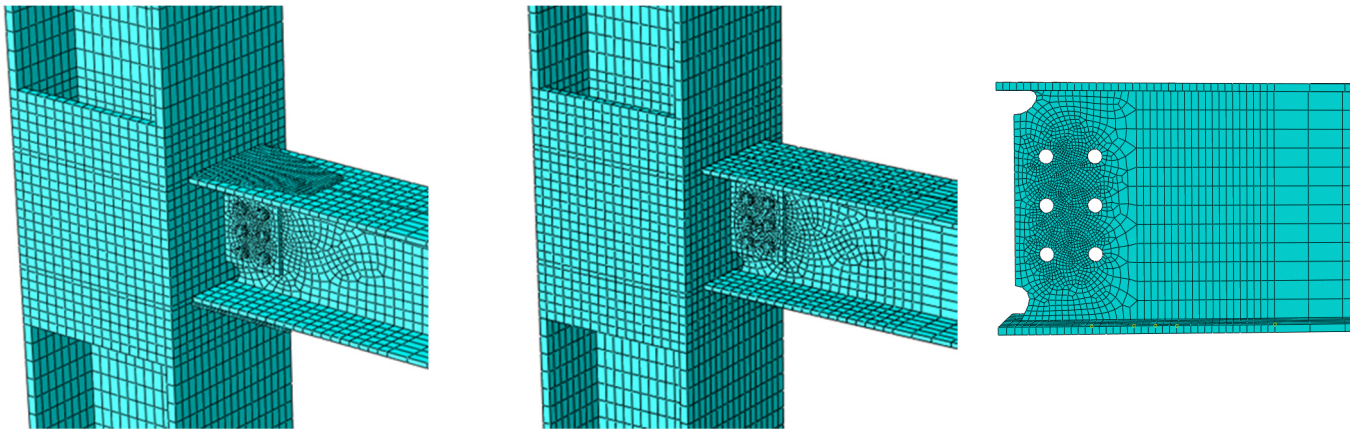

(**a**) (**b**) (**c**)

Figure 3. Three-dimensional finite element local model. (**a**) CP finite element model; (**b**) WCP finite element mode; (**c**) local mesh refinement.

Welded connections were modeled in ABAQUS using the "TIE" command, a common FEA approach for simulating weld behavior. This method simplifies the modeling process, ensuring accurate load transfer and displacement continuity between welded components. It offers a computationally efficient and reliable way to approximate weld performance, particularly for analyzing global structural behavior such as the hysteretic response of RBS connections. Preloading of high-strength bolts was applied based on the JGJ82-2010 [36], using the "bolt load" function in ABAQUS. When preloading is applied, multiple contact interactions are established, including plate-to-beam web, bolt head-to-web, and bolt shank-to-wall interfaces. These interactions were modeled using the "surface-to-surface" contact method, assigning the stiffer surface as the master and the less stiff surface as the slave. Normal contact was "hard", maintaining contact under compression and allowing separation under tension. Tangential contact is governed by Coulomb friction, with a friction factor of 0.44 [37] applied to the bolt connection surfaces.

2.3. ABAQUS Analysis Validation

The CPS-1 Specimen, as shown in Figure 4, originally tested by Wang [38], was chosen for validation purposes. This specimen was fabricated using Q235 steel and incorporated a hybrid bolt–weld connection featuring M20 high-strength bolts. The setup involved a typical simply supported configuration with pinned connections at both beam and column ends, and an axial force of 850 kN was applied to the top of the column. Rectangular cover plates were used for both the top and bottom. The column section was HW 250 × 250 × 9 × 14, with a total length of 2050 mm, while the beam had a length of 1750 mm and a section of HN 300 × 150 × 6.5 × 9. Under displacement-controlled cyclic loading, as described by Wang [38] and conducted following ANSI/AISC 341-05 [35], forces were applied at the beam end. Loading ceased when the bearing capacity dropped to 85% of its maximum value.

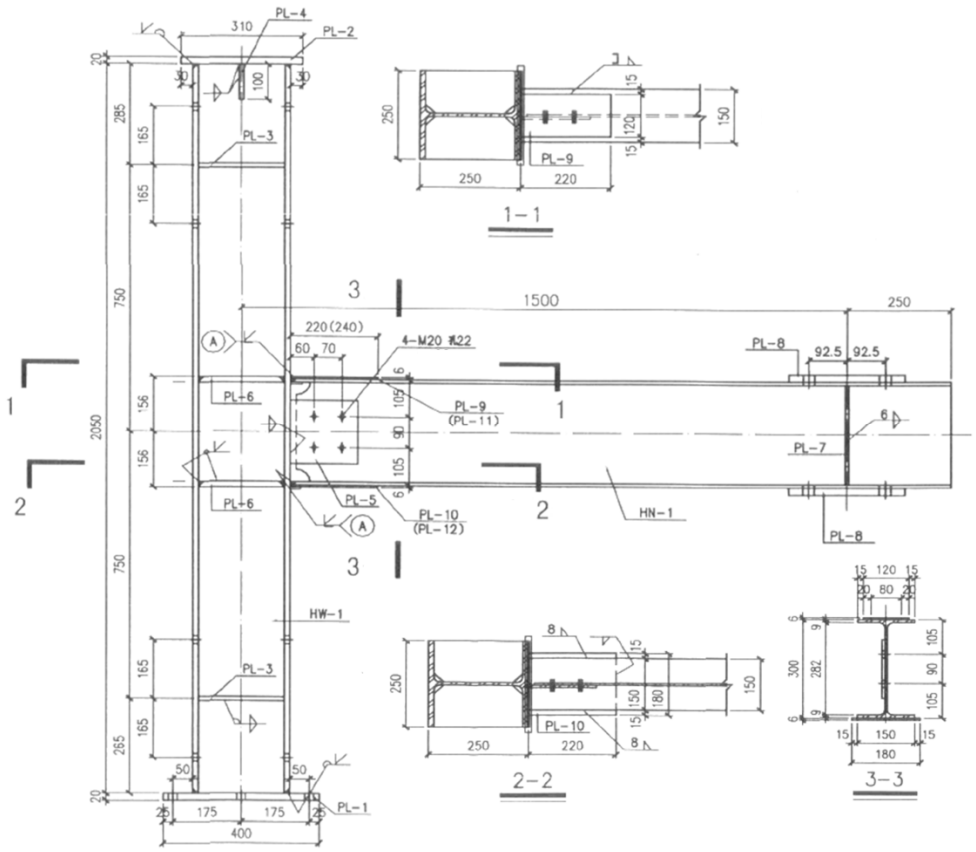

(**a**)

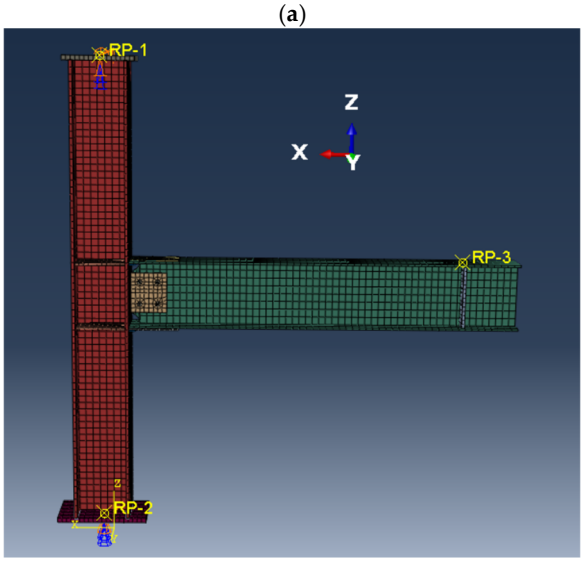

(**b**)

Figure 4. CPS-1 Specimen. (**a**) Schematic diagram of dimensions (Unit: mm); (**b**) ABAQUS model.

The P-Δ hysteresis curve obtained from the CPS-1 experiment is displayed in Figure 5a, while Figure 5b illustrates the corresponding P-Δ curves derived from ABAQUS simulations. Although slight discrepancies exist between the experimental and simulated hysteresis curves, their shapes exhibit high similarity. The peak load recorded during the test was 156.83 kN, whereas the ABAQUS simulation produced a maximum load of 159.5 kN, yielding an error of just 1.7%. The experimental peak load occurred at a beam-end displacement of approximately 56 mm, whereas the simulation reached its maximum load at 58 mm, demonstrating close agreement between the two. The maximum plastic

rotation angle measured in the test was 4.47% rad, compared to 4.75% rad predicted by the simulation, with a difference of 6.1%. The high consistency between the ABAQUS numerical analysis and experimental results indicates that the finite element modeling and analysis in this study are reliable. Additionally, Figure 6 demonstrates that the failure mode observed in the numerical analysis is generally consistent with the experimental results. This methodology can be further employed to investigate the seismic performance of cover-plate connections.

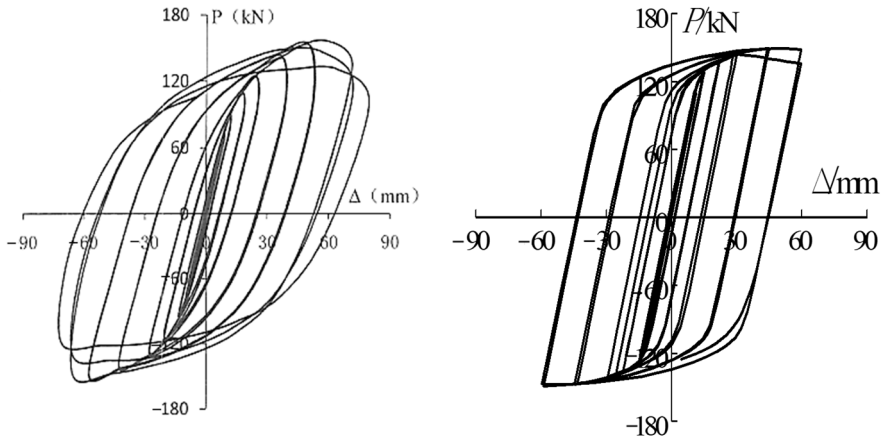

(**a**) (**b**)

Figure 5. P-Δ curves of CPS-1 Specimen. (**a**) Test; (**b**) ABAQUS.

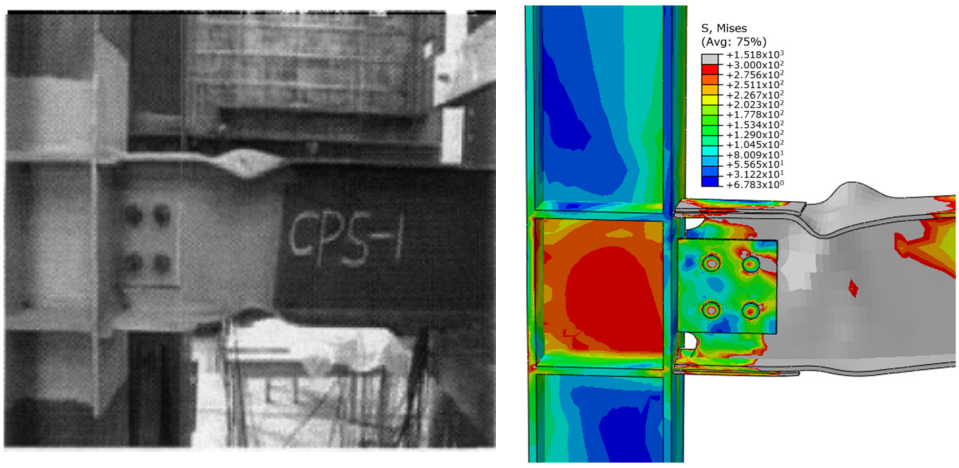

(**a**) (**b**)

Figure 6. Failure modes of CPS-1 Specimen. (**a**) Test; (**b**) ABAQUS.

3. Specimen Design

The columns selected hot-rolled wide-flange H-shape HW 502 × 470 × 20 × 25, and the chosen beams hot-rolled wide-flange H-shape HW 350 × 350 × 12 × 19, hot-rolled middle-flange H-shape HM 390 × 300 × 10 × 16 and HM 340 × 250 × 9 × 14 to build analysis specimens. The research designed different specimens according to the research objectives, as shown in Tables 3 and 4. The research employed three different shapes of top cover plates (trapezoid, wedge, and rectangular) for beams with three different cross-sections, as shown in Figure 7. The researcher uniformly designed the bottom cover plates as rectangular; see the specific data for each specimen as shown in Tables 3 and 4. Explanation of specimen naming: "CP" denotes specimens with cover plates, "WCP" denotes specimens without cover plates, the "CPS" series represents specimens comparing variations in top cover-plate shapes, the "CPL" series represents specimens with varying

lengths of rectangular cover plates, and the "CPT" series represents specimens with varying thicknesses of rectangular cover plates.

Table 3. Details of CP and WCP specimens.

Group No.	Spe.	Beam Size	Beam Length (mm)	Column Size	Column Height (mm)	Cover Plate		
						Size of the Cover Plate		t_{cp}/t_{bf}
						Top	Bottom	
1st group	CP1	HW 350 × 350 × 12 × 19	3000	HW 502 × 470 × 20 × 25	3600	Figure 7(aii)	365 × 370 × 6	0.32
	WCP1	HW 350 × 350 × 12 × 19		HW 502 × 470 × 20 × 25		-	-	-
2nd group	CP2	HM 390 × 300 × 10 × 16	3000	HW 502 × 470 × 20 × 25	3600	Figure 7(bii)	315 × 320 × 6	0.38
	WCP2	HM 390 × 300 × 10 × 16		HW 502 × 470 × 20 × 25		-	-	-
3rd group	CP3	HM 340 × 250 × 9 × 14	3000	HW 502 × 470 × 20 × 25	3600	Figure 7(cii)	265 × 270 × 6	0.24
	WCP3	HM 340 × 250 × 9 × 14		HW 502 × 470 × 20 × 25		-	-	-

Table 4. Full details of CPS, CPL, and CPT series specimens.

Member	Section of Column	Section of Beam	Bottom Cover Plate	Top Cover Plate	Beam Flange Thickness (mm)	Cover-Plate Thickness/Beam Flange Thickness
CPS-1-1	HW 502 × 470 × 20 × 25	HW 350 × 350 × 12 × 19	365 × 370 × 6	Figure 7a	-	-
CPS-1-2			365 × 370 × 6			
CPS1-3			365 × 370 × 6			
CPS-2-1		HM 390 × 300 × 10 × 16	315 × 320 × 6	Figure 7b	-	-
CPS-2-2			315 × 320 × 6			
CPS-2-3			315 × 320 × 6			
CPS-3-1		HM 340 × 250 × 9 × 14	265 × 270 × 6	Figure 7c	-	-
CPS-3-2			265 × 270 × 6			
CPS-3-3			265 × 270 × 6			
CPL-1-1	HW 502 × 470 × 20 × 25	HW 350 × 350 × 12 × 19	335 × 370 × 6	335 × 330 × 6	-	-
CPL-1-2			365 × 370 × 6	365 × 330 × 6		
CPL1-3			395 × 370 × 6	395 × 330 × 6		
CPL-2-1		HM 390 × 300 × 10 × 16	285 × 320 × 6	285 × 280 × 6	-	-
CPL-2-2			315 × 320 × 6	315 × 280 × 6		
CPL-2-3			345 × 320 × 6	345 × 280 × 6		
CPL-3-1		HM 340 × 250 × 9 × 14	235 × 270 × 6	235 × 230 × 6	-	-
CPL-3-2			265 × 270 × 6	265 × 230 × 6		
CPL-3-3			295 × 270 × 6	295 × 230 × 6		
CPT-1-1	HW 502 × 470 × 20 × 25	HW 350 × 350 × 12 × 19	365 × 370 × 4	365 × 330 × 4	19	0.21
CPT-1-2			365 × 370 × 6	365 × 330 × 6	19	0.32
CPT1-3			365 × 370 × 8	365 × 330 × 8	19	0.42
CPT-2-1		HM 390 × 300 × 10 × 16	315 × 320 × 4	315 × 280 × 4	16	0.25
CPT-2-2			315 × 320 × 6	315 × 280 × 6	16	0.38
CPT-2-3			315 × 320 × 8	315 × 280 × 8	16	0.50
CPT-3-1		HM 340 × 250 × 9 × 14	265 × 270 × 4	265 × 230 × 4	14	0.29
CPT-3-2			265 × 270 × 6	265 × 230 × 6	14	0.43
CPT-3-3			265 × 270 × 8	265 × 230 × 8	14	0.57

To facilitate the analysis and description that follows, several geometric parameters are defined as follows: b_{cp} is the width of the cover plate, t_{cp} is the thickness of the cover plate, b_f is the width of the beam flange, t_{bf} is the thickness of the beam flange, l_{cp} is the length of the cover plate, d_b is the beam depth, b_{cp1} is the width of the top cover plate, and b_{cp2} is the width of the bottom cover plate. Several mechanical properties of the joints are defined as follows: R_k represents the initial rotational stiffness. M_y, M_{max}, and M_u denote the yield, peak, and terminated moments, respectively, with corresponding rotational displacements θ_y, θ_{max}, and θ_u. According to FEMA 350 [6], θ_p is defined as the plastic rotation capacity.

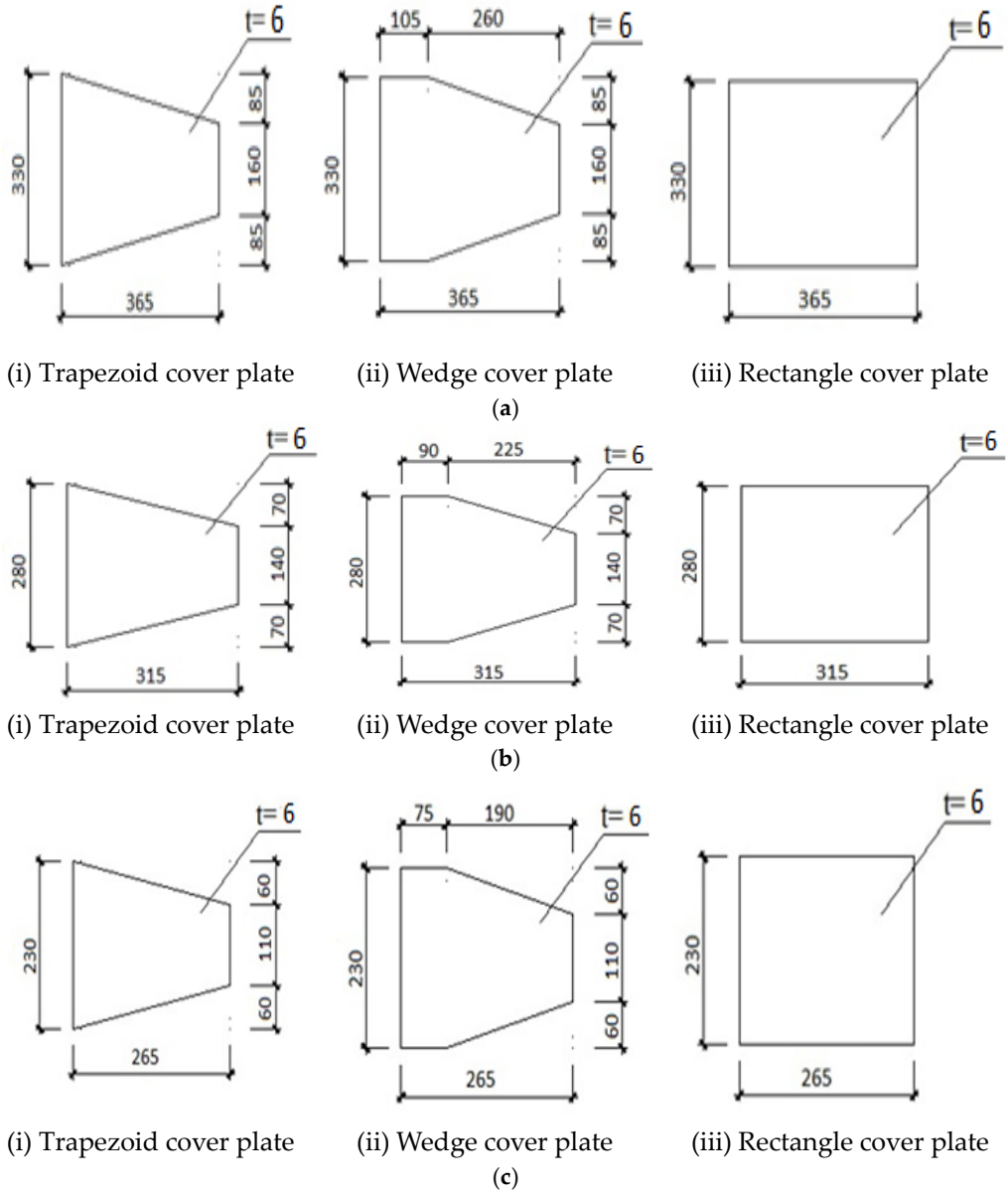

Figure 7. Various cover-plate dimensions (Unit: mm). (**a**) Cover plates for HW 350 × 350 × 12 × 19; (**b**) cover plates for HM 390 × 300 × 10 × 16; (**c**) cover plates for HM 340 × 250 × 9 × 14.

4. Analysis of the Reinforcement Effect of Cover Plates

The failure modes of the three groups of CP and WCP specimens are shown in Figure 8. The hysteresis curves and skeleton curves of the joints are shown in Figures 9–11, respectively. The mechanical properties calculated from the skeleton curves are listed in Table 5.

Table 5. Mechanical properties of CP and WCP specimens.

Group No.	Member	R_k (kN.m/rad)	M_y (kN.m)	θ_y (rad)	M_{max} (kN.m)	θ_{max} (rad)	Mu (kN.m)	θ_u (rad)	θ_p
1st group	CP-1	66,736.88	790	0.021	984.79	0.043	837.08	0.072	0.068
	WCP-1	62,311.39	704	0.020	872.29	0.044	741.45	0.059	0.055
2nd group	CP-2	64,133.85	627	0.014	774.97	0.032	658.72	0.062	0.058
	WCP-2	59,981.84	568	0.015	699.45	0.030	594.53	0.053	0.049
3rd group	CP-3	38,794.91	440	0.023	546.91	0.044	464.88	0.054	0.065
	WCP-3	36,308.14	355	0.016	443.29	0.032	376.79	0.054	0.049

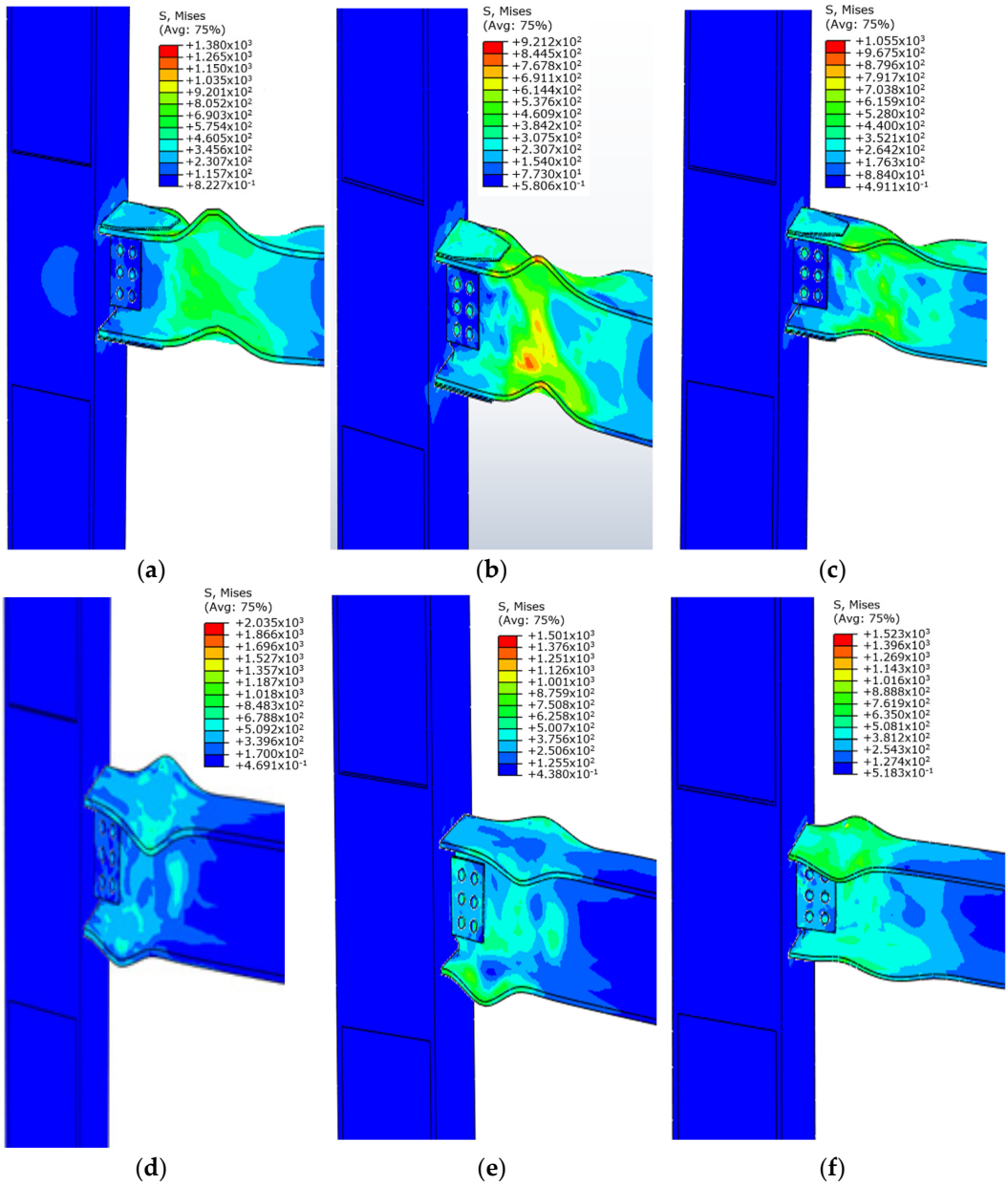

Figure 8. Failure modes of CP and WCP specimens. (**a**) CP-1; (**b**) CP-2; (**c**) CP-3; (**d**) WCP-1; (**e**) WCP-2; (**f**) WCP-3.

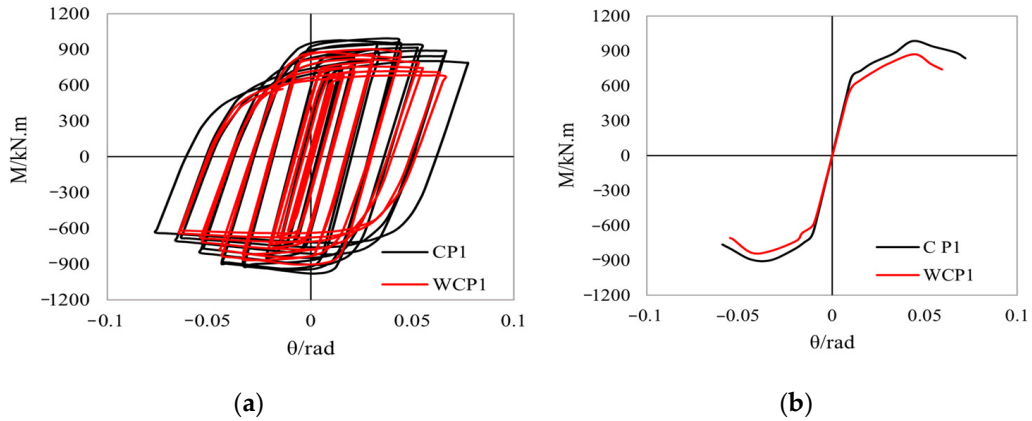

Figure 9. M-θ curves for the 1st group. (**a**) Hysteresis curve; (**b**) skeleton curve.

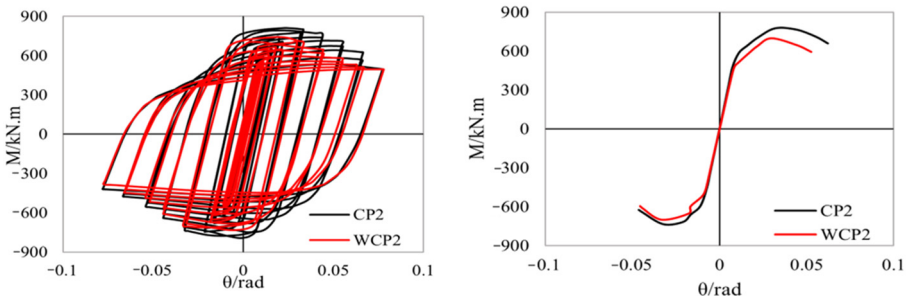

Figure 10. M-θ curves for the 2nd group. (**a**) Hysteresis curve; (**b**) skeleton curve.

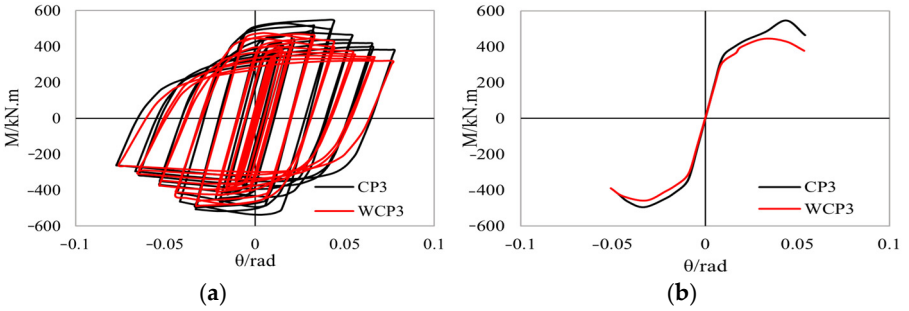

Figure 11. M-θ curves for the 3rd group. (**a**) Hysteresis curve; (**b**) skeleton curve.

As shown in Figure 8, compared with the plastic hinge formation locations in the corresponding WCP specimens, all CP joints enable the beam to form plastic hinges at the outer ends of the cover plates. This indicates that, despite the widened beam flanges, the appropriate configuration of cover plates successfully achieved the intended relocation of plastic hinges. Notably, in the CP-3 specimen, the cover-plate thickness was less than one-fourth of the beam flange thickness, yet it still effectively shifted the plastic hinge outward.

Figures 9–11 illustrate the hysteresis and skeleton curves for CP and WCP specimens. Through the comparison of the hysteresis curves, it can be observed that the curves of the CP specimens are more pronounced than those of the corresponding WCP specimens, indicating that the CP specimens have greater energy dissipation capacity. The comparison of the skeleton curves shows that the elastic stiffness of the CP specimens is similar to that of the corresponding WCP specimens, and the yield rotational deformation is also close. However, the three load indicators (yield moment, peak moment, and terminated moment) of the CP specimens are all higher than those of the corresponding WCP specimens, and the terminated rotational deformation is larger. These results indicate that the CP specimens have better load-bearing capacity and ductility than the WCP specimens, demonstrating that the cover-plate reinforced connection, as one of the post-Northridge connections, has excellent seismic performance.

M_y, M_{max}, and M_u can be calculated through the skeleton curve. Calculations of θ_y, θ_{max}, and θ_u are similar to calculations of the displacements described by Shim et al. [39]. The calculation method for θ_p follows the procedure from the author's previous research [16]. The calculated data for each parameter of the joints are listed in Table 5. Data in Table 5 show that the initial rotational stiffness of the three CP specimen groups increased by approximately 7% on average compared to the WCP specimens. The yield moment My, a key design control parameter, showed an average increase of about 15%. However, in terms of plastic rotational capacity θ_p, which measures the seismic ductility of the joints, the CP specimens achieved an average increase of 25% over the WCP specimens. These results reveal that the cover plates and the strengthened joint regions in this study's middle- and wide-flange hot-rolled H-beam joints effectively enhanced load-bearing capacity and

improved seismic ductility, demonstrating high ductility and load-bearing capacity characteristics [40]. The improvement in the load-bearing capacity and ductility of the cover-plate reinforced joints compared to those without cover plates primarily results from the cover plate transferring the plastic hinge outside the beam–column connection, reducing stress concentration and enhancing both load-bearing capacity and ductility. Additionally, the cover plate increases the stiffness and stability of the joint, reducing local buckling and instability while improving the overall bending capacity and delaying yielding and failure. As a result, the cover plate significantly enhances the joint's load-bearing capacity and ductility, improving the joints' seismic performance.

5. Effect Parameters Analysis of Cover Plates and Discussion

5.1. The Influences of Top Cover-Plate Shape

To facilitate welding, the top cover plate is designed to be narrower than the top flange, while the bottom cover plate is generally wider than the bottom flange. There are three types of top cover plates—trapezoidal, wedge, and rectangular—whereas the bottom cover plate is typically rectangular. To examine the effects of top cover-plate shape on the cyclic response of cover-plate connections, three group CPS series of joints were utilized to analyze the effects (shown in Table 4). The geometric dimensions of the three top cover-plate types are provided in Figure 7. The lower cover plates are all rectangular, with dimensions listed in Table 4.

The failure modes of CPS series joints are illustrated in Figure 12, and the analysis results are summarized in Table 6. As shown in Figure 12 and Table 6, the variation in the top cover-plate shape had a minimal impact on initial rotational stiffness (the average fluctuation amplitude is less than ±1%), load-bearing capacity (the average fluctuation amplitude is less than ±5%), and ductility (the average fluctuation amplitude of θ_p is about ±5%). Additionally, all three group joints' maximum plastic rotation angles exceeded 0.03 rad, meeting FEMA 267 [29]. Therefore, altering the shape of the top cover plate had minimal impact on the mechanical behavior of cover-plate joints, whether the joints used I-section columns with middle-flange or wide-flange beams. However, trapezoidal and wedge-shaped cover plates can reduce the total length of filet welds and lessen the welding heat effect on the beam flange steel. Conversely, rectangular cover plates offer greater ease of fabrication.

Table 6. Numerical analysis results of all CPS, CPL, and CPT series specimens.

Member	R_k (kN.m/rad)	M_y (kN.m)	θ_y (rad)	M_{max} (kN.m)	θ_{max} (rad)	M_u (kN.m)	θ_u (rad)	θ_p (rad)
CPS-1-1	66,583.86	805	0.0216	971.05	0.0423	825.39	0.073	0.069
CPS-1-2	66,736.88	790	0.0212	984.79	0.0434	837.08	0.072	0.068
CPS1-3	66,995.35	728	0.0152	922.89	0.0432	784.46	0.069	0.065
CPS-2-1	64,001.49	623	0.0142	769.54	0.0445	654.11	0.065	0.061
CPS-2-2	64,133.85	627	0.0142	774.97	0.0319	658.72	0.062	0.058
CPS-2-3	64,358.96	632	0.0143	779.03	0.0425	662.18	0.064	0.060
CPS-3-1	38,721.33	455	0.022	539.72	0.0444	458.76	0.055	0.051
CPS-3-2	38,794.91	440	0.02285	546.91	0.0440	464.88	0.054	0.050
CPS-3-3	38,937.06	430	0.01885	523.5	0.0446	444.97	0.051	0.047
CPL-1-1	66,677.97	720	0.0152	921.81	0.0445	783.54	0.067	0.063
CPL-1-2	66,995.35	728	0.015	922.89	0.0432	784.46	0.069	0.065
CPL1-3	67,306.95	820	0.0197	976.31	0.0445	829.86	0.060	0.056
CPL-2-1	64,011.88	628	0.0145	768.2	0.0308	652.97	0.055	0.050
CPL-2-2	64,358.96	635	0.015	779.03	0.0425	662.18	0.064	0.060
CPL-2-3	64,700.05	640	0.0144	788.19	0.0437	669.97	0.068	0.064
CPL-3-1	38,677.23	405	0.0177	508.08	0.0445	431.87	0.050	0.046
CPL-3-2	38,937.06	430	0.0189	523.5	0.0446	444.97	0.051	0.047
CPL-3-3	39,194.10	395	0.0143	497.41	0.0438	422.8	0.055	0.051

Table 6. *Cont.*

Member	R_k (kN.m/rad)	M_y (kN.m)	θ_y (rad)	M_{max} (kN.m)	θ_{max} (rad)	M_u (kN.m)	θ_u (rad)	θ_p (rad)
CPT-1-1	65,600.07	712	0.014	889.75	0.0438	756.29	0.061	0.056
CPT-1-2	66,263.70	724	0.0148	919.34	0.0445	781.44	0.064	0.050
CPT-1-3	66,860.34	725	0.0148	921.46	0.0427	783.24	0.073	0.048
CPT-2-1	63,091.55	610	0.0132	755.72	0.0446	642.36	0.064	0.059
CPT-2-2	63,695.87	608	0.0129	756.95	0.0332	643.41	0.05	0.056
CPT-2-3	64,228.23	612	0.0131	763.67	0.0333	649.44	0.056	0.051
CPT-3-1	38,198.82	415	0.0191	519.99	0.0446	441.99	0.056	0.052
CPT-3-2	38,548.34	388	0.0146	482.89	0.044	410.46	0.053	0.048
CPT-3-3	38,850.70	436	0.0186	514.58	0.0436	437.40	0.052	0.048

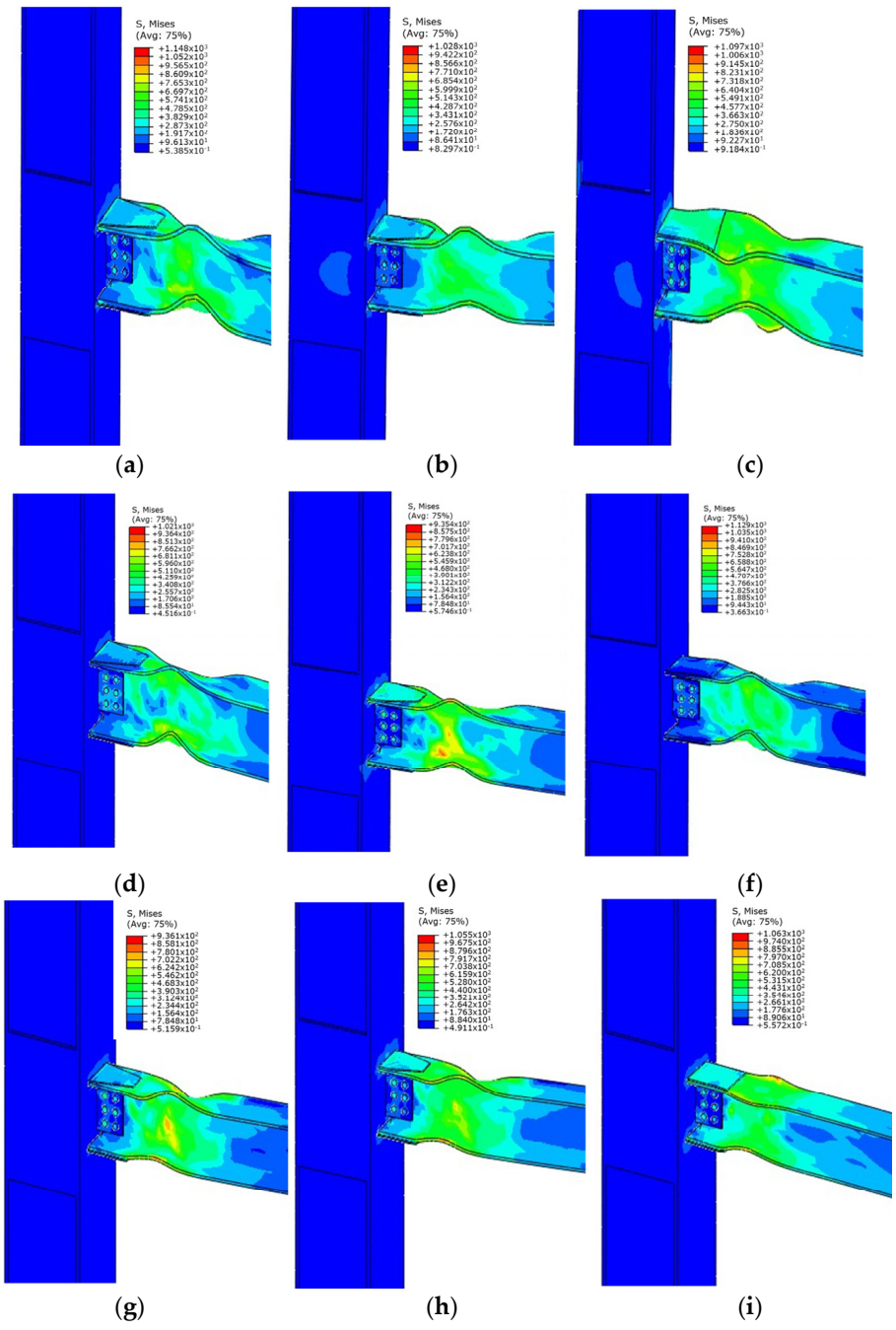

Figure 12. Failure modes of CPS series joints. (**a**) CPS-1-1; (**b**) CPS-1-2; (**c**) CPS-1-3; (**d**) CPS-2-1; (**e**) CPS-2-2; (**f**) CPS-2-3; (**g**) CPS-3-1; (**h**) CPS-3-2; (**i**) CPS-3-3.

5.2. The Influences of Cover-Plate Length

FEMA 267 [29] recommends the minimum cover-plate length be at least half of the beam depth for cover-plate moment connections, and it is the same as BS EN 1998-3 [12]. JGJ99-2015 [13] recommends a range of 0.5 to 0.75 times the beam depth. To better understand the mechanical behavior of cover-plate connections with varying cover-plate lengths, series joints were designed, as shown in Table 4, as follows: CPL-1: l_{cp} = (0.96~1.12) d_b, CPL-2: l_{cp} = (0.73~0.88) d_b, and CPL-3: l_{cp} = (0.69~0.87) d_b. Following the conclusions in Section 5.1, the rectangular cover plates were selected for all specimens for convenience, with specific details provided in Table 4.

The failure modes of the CPL series joints are illustrated in Figure 13, with numerical analysis results summarized in Table 6. As shown in Figure 13, plastic hinges were successfully formed in the CPL-2 and CPL-3 series specimens outside the cover plate. In contrast, for the CPL-1 series specimens, except for CPL-1-1, the cover plates of CPL-1-2 and CPL-1-3 were located within the plastic hinge region and exhibited significant deformation. A cover plate that is too long may extend into the plastic hinge region of the beam, causing considerable deformation. This is mainly due to the excessive bending moment in the plastic hinge region, which leads to bending and local yielding. Additionally, stress concentration and deformation amplification effects are intensified. Furthermore, an overly long cover plate may lead to local buckling and uneven plastic deformation, further increasing the deformation. Therefore, for cover-plate connections using hot-rolled H-shaped beams with middle or wide flanges, the observations indicate that the cover-plate length should not exceed 0.9 times the beam depth. Additionally, based on the analysis data for the CP-2 and CP-3 series specimens in Table 6, it was found that variations in cover-plate length (within 0.90 times the beam depth) had a minor effect on the initial rotational stiffness and bearing capacity of the joints, with fluctuations within ±3%. However, as the length increased, the plastic rotational capacity θ_p increased significantly, with an improvement exceeding 10%. This indicates that changes in cover-plate length have a notable impact on the seismic ductility of the joints.

Based on the observations and data analysis, a reasonable cover-plate length, 0.70~0.90 times the beam depth, is recommended for better ductility and plastic rotation capacity.

5.3. The Influences of Cover-Plate Thickness

For cover-plate connections, BS EN 1998-3 [12] requires the cover-plate thickness to be 1.2 times the beam flange thickness, while JGJ99-2015 [13] specifies that it should be no less than the beam flange thickness. FEMA 267 [29] requires that the combined thickness of the cover plate and beam flange must exceed twice the beam flange thickness but remain less than the column flange thickness. However, from the perspective of ensuring a strong-column–weak-beam mechanism, the FEMA 267 [29] requirement that the combined thickness of the cover plate and beam flange must not exceed the thickness of the column flange is more critical. This implies that the BS EN 1998-3 [12] and JGJ99-2015 [13] are not comprehensive enough, especially when the cover-plate thickness must be smaller than the beam flange thickness. In fact, China's national architectural design standard atlas 16G519 [41] only specifies that the cover-plate thickness should be greater than or equal to 6mm without following the provisions of the JGJ99-2015 [13]. Therefore, all specimens designed in this study adhered to the principle of FEMA 267 [29]. Notably, the CPS and CPL series specimens analyzed earlier demonstrated an ideal plastic hinge failure mode in the beams. This means that using a cover plate much thinner than the beam flange thickness can still ensure the characteristics of the reinforced connection. The beam plastic hinge is easily formed and located far from the column flange.

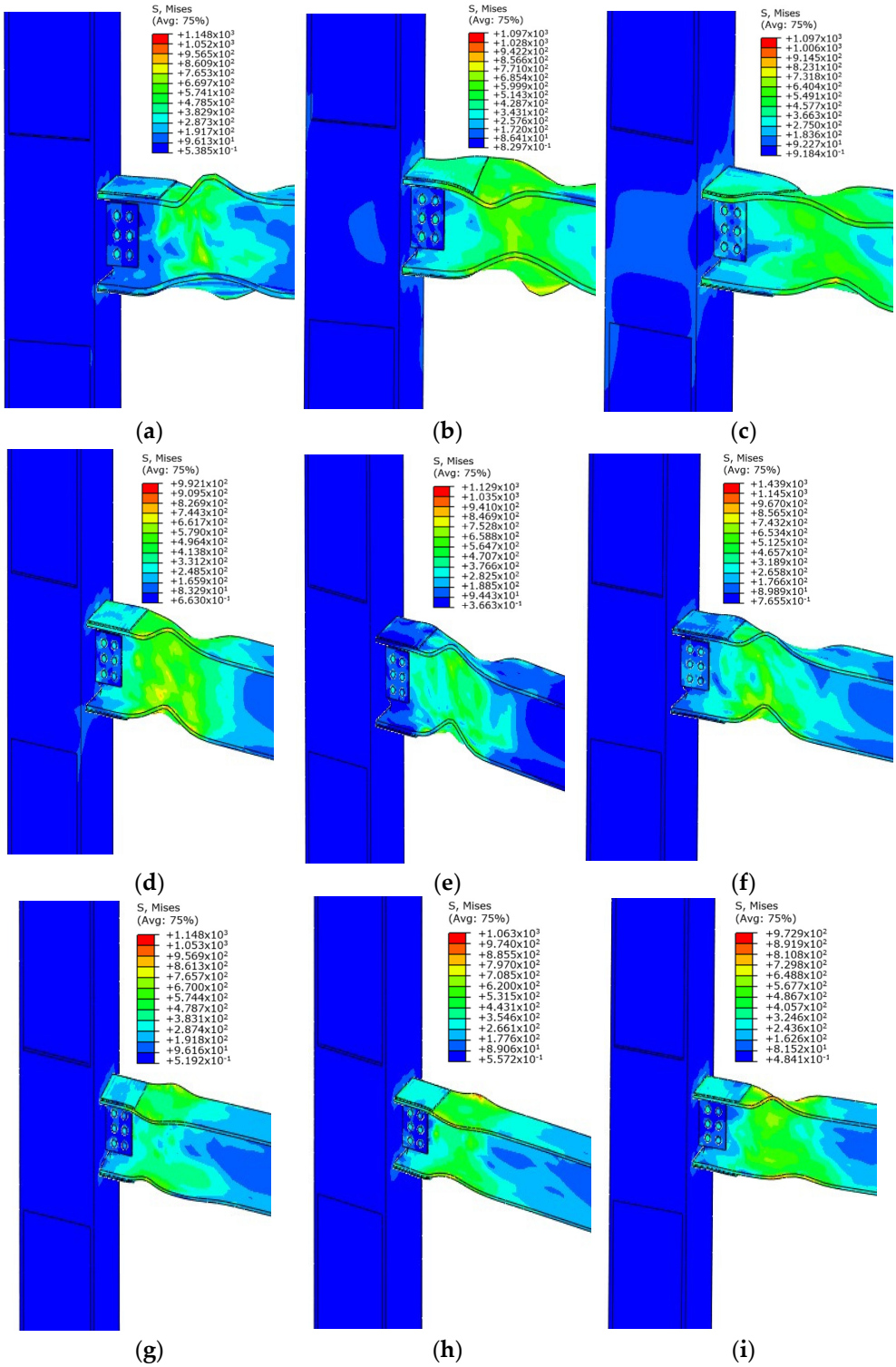

Figure 13. Failure modes of CPL series joints. (**a**) CPL-1-1; (**b**) CPL-1-2; (**c**) CPL-1-3; (**d**) CPL-2-1; (**e**) CPL-2-2; (**f**) CPL-2-3; (**g**) CPL-3-1; (**h**) CPL-3-2; (**i**) CPL-3-3.

From another perspective, this suggests that the thickness requirements for cover plates in BS EN 1998-3 [12] and JGJ99-2015 [13] may be overly conservative. In practice, excessively thick plates necessitate very thick groove welds to connect the beam flange ends to the column flanges, increasing the risk of weld defects and potential fracture failure during earthquakes. Therefore, the CPT series specimens were designed to explore the minimum feasible thickness for cover plates, as detailed in Table 4.

Increasing the cover-plate thickness enhances the connection's initial rotational stiffness and bearing capacity. However, its effects on joint plastic rotation capacity require quantification through numerical analysis. As shown in Figure 14, the plastic hinge of specimen CPT-1-1 extended into the cover plate, while that of CPT-2-1 slightly reached the edge. The plastic hinges, for others, were formed outside the cover plate. By examining the ratio of cover-plate thickness to beam flange thickness (Table 4), it was found that when the cover-plate thickness is greater than or equal to 0.3 times the beam flange thickness, the combined thickness of the cover plate and beam flange is less than the column flange thickness, and cover-plate connections can achieve the performance of reinforced connections for hot-rolled H-shaped beams with middle or wide flanges. This significantly enhances the ability to extend plastic hinge formation outward. Additionally, the data in Table 6 show that for the CPT specimens in this study, the increase in cover-plate thickness improved the initial rotational stiffness and bearing capacity by less than 5%, which can be considered negligible. The joint's plastic rotational capacity reductions are more than 5%, warranting consideration of its impact. The mechanism behind this phenomenon can be explained as follows: increasing the cover-plate thickness increases the local stiffness of the beam end, thereby enhancing the connection's load-bearing capacity. However, as the stiffness increases, the plastic deformation capacity of both the cover plate and the beam end is restricted. Although the plastic hinge is pushed out to the cover plate, this also reduces plastic rotation capacity. In contrast, a thinner cover plate offers less deformation constraint due to its lower stiffness, causing the cover-plate region to undergo plastic deformation prematurely. This prevents the plastic hinge from moving outward while reducing the load-bearing capacity.

However, the plastic rotational capacity of all specimens exceeded 0.03 rad, which is the minimum rotational capacity requirement specified by FEMA 267 [29]. Based on the observations and data analysis, and considering the practical experience from the Chinese standard drawing set 16SG519 [41], it is recommended that the minimum thickness of the cover plate be 0.3 times the flange thickness of the beam, not less than 6mm. Additionally, the total thickness of the cover plate and beam flange should not exceed the thickness of the column flange, considering the balance between the connection's stiffness and ductility.

5.4. Discussion

This study presents a comprehensive analysis of cover-plate connections for hot-rolled H-shaped beams with middle or wide flanges, comparing the results with existing design guidelines, including FEMA 267 [29], BS EN 1998-3 [12], JGJ99-2015 [13], and China's national standard 16SG519 [41]. This research provides valuable insights into the behavior of cover-plate connections, particularly regarding the influences of cover-plate length and thickness.

1. Cover-Plate Length:

The study's findings suggest that cover-plate length significantly impacts the connection's seismic ductility. Specifically, the research recommends a cover-plate length of up to 0.90 times the beam depth to achieve optimal ductility and bearing capacity, aligning with the observations that cover plates longer than this can induce excessive deformation and stress concentration. This is consistent with the guidelines of FEMA 267 [29], BS EN 1998-3 [12], and JGJ99-2015 [13], which suggest a minimum cover-plate length of at least half the beam depth. However, the recommended cover-plate length of 0.70~0.90 times the beam depth in this study exceeds the upper limit of 0.75 times the beam depth specified by BS EN 1998-3 [12] and JGJ99-2015 [13]. This breakthrough is particularly suitable for hot-rolled H-shaped beams with middle or wide flanges, as it allows for better plastic rotation

capacity and seismic ductility, which are critical for enhancing the overall performance of the connection.

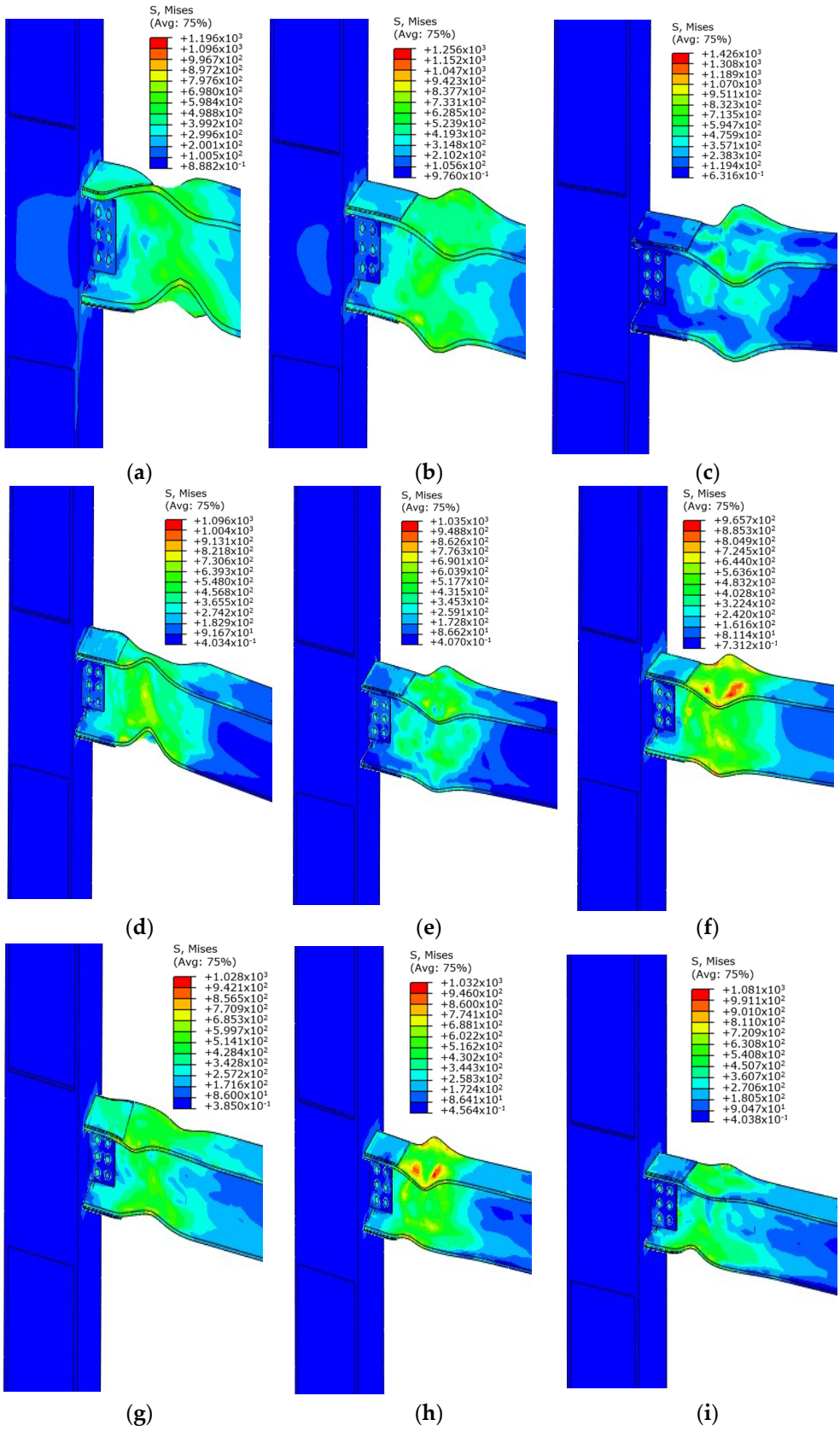

Figure 14. Failure modes of CPT series joints. (**a**) CPT-1-1; (**b**) CPT-1-2; (**c**) CPT-1-3; (**d**) CPT-2-1; (**e**) CPT-2-2; (**f**) CPT-2-3; (**g**) CPT-3-1; (**h**) CPT-3-2; (**i**) CPT-3-3.

2. Cover-Plate Thickness:

The research challenges the conservatism of current design standards regarding cover-plate thickness. While BS EN 1998-3 [12] and JGJ99-2015 [13] specify that the cover-plate thickness should be 1.2 times or 1.0 times the beam flange thickness, the study shows that a thinner cover plate, as long as it is at least 0.3 times the beam flange thickness and no less than 6mm, can still effectively reinforce the connection without compromising its performance. This suggests that the prescribed thickness in current standards may be overly conservative, leading to unnecessary material use and potential fabrication challenges.

The recommendation for cover-plate thickness in this study, although deviating from the provisions of BS EN 1998-3 [12] and JGJ99-2015 [13], aligns with FEMA 267 [29] and 16SG519 [41] and may be more suitable for the connections of middle-flange and wide-flange hot-rolled H-shaped steel beams studied in this research.

6. Conclusions

This research presents a comprehensive investigation into the impact of cover-plate geometry on the mechanical performance of steel frame connections, with a specific focus on joints using middle-flange and wide-flange H-shapes. The study contributes novel insights into the design of steel frame connections, particularly in improving seismic resilience and joint ductility. Key findings include the following:

1. Adopting cover-plate reinforced connections can effectively shift plastic hinge formation outward in frame connections using middle-flange or wide-flange H-shaped steel beams. This strategy significantly enhances the seismic performance and ductility of the joint. Compared to WCP specimens, CP specimens increased ductility by approximately 25% and improved initial rotational stiffness and yield moment by 7% and 15%, respectively.
2. Adjusting the length of the cover plate impacts seismic ductility. A reasonable cover-plate length, 0.70~0.90 times the beam depth, is recommended for better ductility and plastic rotation capacity, although it exceeds the upper limit of 0.75 times the beam depth specified by BS EN 1998-3 and JGJ99-2015.
3. The cover-plate thickness plays a crucial role in seismic ductility. This study recommends that the cover-plate thickness be at least 0.3 times the beam flange thickness (not less than 6mm) and that the combined thickness of the cover plate and beam flange not exceed the column flange thickness to maintain a balance between connection stiffness and ductility, even though this does not comply with the provisions of BS EN 1998-3 and JGJ99-2015.

For further investigating the application of cover-plate connections in modern steel frames, future research could focus on the performance of cover-plate reinforced connections specifically for middle- and wide-flange H-shaped steel beams, considering the effects of slab interaction under various loading conditions, to further refine design guidelines and enhance their applicability.

Author Contributions: Conceptualization, L.L.; software, O.Z.Y.A.-a.; validation, O.Z.Y.A.-a., S.M.A.A.A.-S. and B.L.; resources, L.L.; writing—original draft preparation, O.Z.Y.A.-a. and L.L.; writing—review and editing, L.L., O.Z.Y.A.-a., S.M.A.A.A.-S. and B.L.; project administration, L.L.; funding acquisition, L.L. All authors have read and agreed to the published version of the manuscript.

Funding: This research was funded by the Nature Science Foundation of China (NSFC), grant number 51278061.

Data Availability Statement: The original contributions presented in the study are included in the article, further inquiries can be directed to the corresponding author.

Conflicts of Interest: The authors declare that they have no conflict of interests.

References

1. Kinki, A.I.J. *Reconnaissance Report on Damage to Steel Building Structures Observed from the 1995 Hyogoken-Nanbu Earthquake*; Steel Committee of Kinki Branch, Architectural Institute of Japan: Osaka, Japan, 1995.
2. Mahin, S.A. Lessons from damage to steel buildings during the Northridge earthquake. *Eng. Struct.* **1998**, *20*, 261–270. [CrossRef]
3. Muguruma, H.; Nishiyama, M.; Watanabe, F. Lessons learned from the Kobe earthquake—A Japanese perspective. *Pci J.* **1995**, *40*, 28–42. [CrossRef]
4. Malley, J.O.; Carter, C.J.; Saunders, C.M. Seismic design guidelines and Provisions for steel-framed buildings: FEMA 267/267A and 1997 AISC Seismic Provisions. *Earthq. Spectra* **2000**, *16*, 179–203. [CrossRef]
5. Simoncelli, M.; Zucca, M.; Stochino, F. Fire Resistance of Steel Rack Frames: Assessment, Reinforcement and Collapse Mitigation Strategies. *Fire Technol.* **2024**, 1–23. [CrossRef]
6. *FEMA-350*; Recommended Seismic Design Criteria for New Steel Moment-Frame Buildings. FEMA: Washington, DC, USA, 2000.
7. Nakashima, M.; Roeder, C.W.; Maruoka, Y. Steel moment frames for earthquakes in United States and Japan. *J. Struct. Eng.* **2000**, *126*, 861–868. [CrossRef]
8. Engelhardt, M.D.; Sabol, T.A. Reinforcing of steel moment connections with cover plates: Benefits and limitations. *Eng. Struct.* **1998**, *20*, 510–520. [CrossRef]
9. Kim, T.; Whittaker, A.S.; Gilani, A.S.J.; Bertero, V.V.; Takhirov, S.M. Experimental evaluation of plate-reinforced steel moment-resisting connections. *J. Struct. Eng.* **2002**, *128*, 483–491. [CrossRef]
10. *FEMA-351*; Recommended Seismic Evaluation and Upgrade Criteria for Existing Welded Steel Moment-Frame Buildings. FEMA: Washington, DC, USA, 2000.
11. *FEMA-355D*; State of the Art Report on Connection Performance. FEMA: Sacramento, CA, USA, 2000.
12. *BS EN 1998-3*; Eurocode 8: Design of Structures for Earthquake Resistance Part 3: Assessment and Retrofitting of Buildings. British Standards Institution: London, UK, 2006.
13. *JGJ99-2015*; Technical Specification for Steel Structures of Tall Buildings. China Architecture & Building Press: Beijing, China, 2015.
14. *GB 50011-2010*; Code for Seismic Design of Buildings. China Architecture & Building Press: Beijing, China, 2010.
15. Lu, L.; Xu, Y.; Zheng, H. Investigation of composite action on seismic performance of weak-axis column bending connections. *J. Constr. Steel Res.* **2017**, *129*, 286–300. [CrossRef]
16. Lu, L.; Xu, Y.; Lim, J.B.P. Mechanical performance of a new I-section weak-axis column bending connection. *Steel Compos. Struct.* **2018**, *26*, 31–44.
17. Lu, L.; Xu, Y.; Zheng, H.; Lim, J.B.P. Cyclic response and design procedure of a weak-axis cover-plate moment connection. *Steel Compos. Struct.* **2018**, *26*, 329–345.
18. Chen, X.; Shi, G. Experimental study on seismic behaviour of cover-plate joints in high strength steel frames. *Eng. Struct.* **2019**, *191*, 292–310. [CrossRef]
19. Jiang, S.; Shi, G.; Zhang, N.; Zhao, H.; Sun, T. Experimental study on seismic behavior of cover-plate connections between steel beams and high strength steel box columns. *Thin-Walled Struct.* **2023**, *193*, 111208. [CrossRef]
20. Casita, C.B.; Suswanto, B.; Iranata, D.; Matsumura, M. Numerical Investigation to Assess the Cyclic Performance of RBS Connection using Cover Plates. *E3S Web Conf.* **2023**, *434*, 02017. [CrossRef]
21. Meng, B.; Du, Q.; Li, F.; Duan, S.; Li, L. Seismic performance of steel connections with double-leg energy dissipation cover plates. *Structures* **2022**, *43*, 1945–1961. [CrossRef]
22. Ribeiro, T.; Bernardo, L.; Carrazedo, R.; De Domenico, D. Eurocode-compliant topology optimisation and analysis of a steel cover-plate in a splice moment connection. *Mater. Today Proc.* **2022**, *65*, 1056–1063. [CrossRef]
23. Nassiraei, H. Probabilistic analysis of strength in retrofitted X-Joints under tensile loading and fire conditions. *Buildings* **2024**, *14*, 2105. [CrossRef]
24. Zhai, S.Y.; Lyu, Y.F.; Cao, K.; Li, G.Q.; Wang, W.Y.; Chen, C. Experimental study on bolted-cover plate corner connections for column-supported modular steel buildings. *J. Constr. Steel. Res.* **2022**, *189*, 107060. [CrossRef]
25. Zhai, S.Y.; Lyu, Y.F.; Cao, K.; Li, G.Q.; Wang, W.Y.; Chen, C. Experimental-numerical investigation and design of bolted-cover plate connections under bending for modular steel buildings. *J. Build. Eng.* **2023**, *75*, 107057. [CrossRef]
26. Cao, K.; Zhai, S.Y.; Lyu, Y.F.; Li, G.Q.; Wang, W.Y.; Chen, C. Working mechanism evaluations of full-scale joints with bolted-cover plate connection for modular steel buildings. *Thin-Walled Struct.* **2024**, *199*, 111772. [CrossRef]
27. Deng, E.F.; Lian, J.Y.; Zhang, Z.; Qian, H.; Zhang, G.C.; Zhang, P.; Sheikh, S.A. Axial mechanical behavior of an innovative liftable connection for modular steel construction. *Thin-Walled Struct.* **2023**, *182*, 110256. [CrossRef]
28. Deng, E.F.; Wang, Y.H.; Zong, L.; Zhang, Z.; Zhang, J.F. Seismic behavior of a novel liftable connection for modular steel buildings: Experimental and numerical studies. *Thin-Walled Struct.* **2024**, *197*, 111563. [CrossRef]

29. *FEMA-267*; Interim Guidelines: Evaluation, Repair, Modification and Design of Steel Moment Frames, Report No. SAC-95-02. FEMA: Washington, DC, USA, 1995.
30. Gemechu, T.D.; Lu, L. Analysis of Factors Affecting the Seismic Performance of Widened Flange Connections in Mid-Flange H-Beams and Box Columns. *Buildings* **2024**, *14*, 3170. [CrossRef]
31. Valente, M. Numerical investigations of steel beam-to-column connections with reinforcing plates. *Appl. Mech. Mater.* **2012**, *234*, 78–83. [CrossRef]
32. Valente, M.; Castiglioni, C.A.; Kanyilmaz, A. Dissipative devices for earthquake resistant composite steel structures: Bolted versus welded solution. *Bull. Earthq. Eng.* **2016**, *14*, 3613–3639. [CrossRef]
33. Nie, W.; Lu, L.; Li, R.; Hao, H.; Luo, T. Global buckling investigation of T-shaped built-up columns composed of two hot-rolled H-shapes. *Structures* **2023**, *58*, 105485. [CrossRef]
34. Katiana, K.; Apostolos, K.; Olympia, P. Numerical investigation of weak axis I profile connections. In Proceedings of the 9th Hellenic National Conference on Steel Structures, Larissa, Thessaly, Greece, 5–7 October 2017.
35. *ANSI/AISC 341-05*; Seismic Provisions for Structural Steel Buildings. American Institute of Steel Construction: Chicago, IL, USA, 2005.
36. *JGJ 82-2011*; Technical Specification for High Strength Bolt Connections of Steel Structures. China Architecture & Building Press: Beijing, China, 2011.
37. Lu, L.; Zhu, P.; Ding, S.; Ma, Z.; Li, R.; Nie, S.; Wang, W.; Raftery, G.M. Impact of anti-corrosion coatings and maintenance on high-strength bolt friction connections in C4 marine environment. *Structures* **2024**, *68*, 107098. [CrossRef]
38. Wang, P. Experimental Evaluation of Flange-Plate Reinforced and Cover-Plate Reinforced Steel Moment-Resistance Connections. Master's Thesis, Qingdao University of Technology, Qingdao, China, 2009.
39. Shim, H.J.; Lee, E.T.; Kim, S.B.; Kim, S.S. Development and performance evaluation of weak-axis column bending connections for advanced constructability. *Int. J. Steel Struct.* **2014**, *14*, 369–380. [CrossRef]
40. Lu, L.; Zhang, J.; Zhang, G.; Peng, H.; Liu, B.; Hao, H. The Influence of Box-Strengthened Panel Zone on Steel Frame Seismic Performance. *Buildings* **2023**, *13*, 3042. [CrossRef]
41. *16G519*; Detail Drawings of Steel Structure Joints for Multi-Story and High-Rise Civil Buildings. China Planning Press: Beijing, China, 2016.